Ceramic Materials in Na$_2$O-CaO-P$_2$O$_5$ System, Obtained via Heat Treatment of Cement-Salt Stone Based on Powder Mixture of Ca$_3$(C$_6$H$_5$O$_7$)$_2$ · 4H$_2$O, Ca(H$_2$PO$_4$)$_2$ · H$_2$O and NaH$_2$PO$_4$

Otabek U. Toshev [1,*], Tatiana V. Safronova [1,2], Tatiana B. Shatalova [1,2] and Yulia S. Lukina [3]

[1] Department of Materials Science, Lomonosov Moscow State University, Building, 73, Leninskie Gory, 1, Moscow 119991, Russia

[2] Department of Chemistry, Lomonosov Moscow State University, Building, 3, Leninskie Gory, 1, Moscow 119991, Russia

[3] National Medical Research Center for Traumatology and Orthopedics Named after N.N. Priorov, Priorova 10, Moscow 127299, Russia

[*] Correspondence: toshevou@my.msu.ru; Tel.: +7-977-522-50-62

Abstract: Ceramic materials in Na$_2$O-CaO-P$_2$O$_5$ system were obtained by firing cement-salt stone made from pastes based on powder mixtures including calcium citrate tetrahydrate Ca$_3$(C$_6$H$_5$O$_7$)$_2$ · 4H$_2$O, monocalcium phosphate monohydrate (MCPM) Ca(H$_2$PO$_4$)$_2$ · H$_2$O and/or sodium dihydrogen phosphate NaH$_2$PO$_4$. The phase composition of the obtained samples of cement-salt stone after adding water, hardening and drying included brushite CaHPO$_4$ · 2H$_2$O, monetite CaHPO$_4$ and also unreacted Ca$_3$(C$_6$H$_5$O$_7$)$_2$ · 4H$_2$O, Ca(H$_2$PO$_4$)$_2$ · H$_2$O and/or NaH$_2$PO$_4$. The phase composition of ceramics in Na$_2$O-CaO-P$_2$O$_5$ system obtained by firing cement-salt stone was formed due to thermal conversion of hydrated salt and heterophase reactions between components presented in samples during firing. The phase composition of ceramic samples based on powder mixture of Ca$_3$(C$_6$H$_5$O$_7$)$_2$ · 4H$_2$O and Ca(H$_2$PO$_4$)$_2$ · H$_2$O after firing at 900 °C included β-calcium pyrophosphate (CPP) β-Ca$_2$P$_2$O$_7$. The phase composition of ceramic samples based on powder mixture of Ca$_3$(C$_6$H$_5$O$_7$)$_2$ · 4H$_2$O, and NaH$_2$PO$_4$ after firing at 900 °C included β-sodium rhenanite β-CaNaPO$_4$. The phase composition of ceramic samples based on powder mixture of Ca$_3$(C$_6$H$_5$O$_7$)$_2$ · 4H$_2$O, Ca(H$_2$PO$_4$)$_2$ · H$_2$O and NaH$_2$PO$_4$ after firing at 900 °C included β-Ca$_2$P$_2$O$_7$, β-CaNaPO$_4$, double calcium-sodium pyrophosphate Na$_2$CaP$_2$O$_7$, and Na-substituted tricalcium phosphate Ca$_{10}$Na(PO$_4$)$_7$. Obtained ceramic materials in Na$_2$O-CaO-P$_2$O$_5$ system including biocompatible and biodegradable phases could be important for treatments of bone tissue defects by means of approaches of regenerative medicine.

Keywords: monocalcium phosphate monohydrate; sodium dihydrogen phosphate; calcium citrate tetrahydrate; cement-salt stone; brushite; monetite; ceramics; calcium pyrophosphate; sodium rhenanite, sodium-substituted tricalcium phosphate, sodium-calcium pyrophosphate

1. Introduction

One of the important areas of modern inorganic materials science is the development of biomaterials based on calcium phosphates that could be used to replace or treat damaged bone tissue [1]. Ideally, the implant should gradually dissolve in the body's environment, while performing its supporting functions, and new bone tissue should form in its place. In this regard, the key characteristic of the biocompatible inorganic material is the property which enables it to resorb in the body's environment. The traditionally used hydroxyapatite Ca$_{10}$(PO$_4$)$_6$(OH)$_2$ (HAP) has the lowest solubility among calcium phosphates [2]. In the case of a regenerative approach to the treatment of bone tissue, bioresorbable phases are introduced into the composition of materials for bone implants. Such materials, compared to HAP, have greater resorption. Among them are Ca$_3$(PO$_4$)$_2$ (tricalcium

phosphate, TCP, Ca/P = 1.5) [3,4], $Ca_2P_2O_7$ (calcium pyrophosphate, CPP, Ca/P = 1) [5,6], $Ca_4P_6O_{19}$ (tromelite, Ca/P = 0,66) [7], $Ca(PO_3)_2$ (calcium polyphosphate, Ca/P = 0.5) [8], Na−substituted tricalcium phosphate $Ca_{10}Na(PO_4)_7$, K−substituted tricalcium phosphate $Ca_{10}K(PO_4)_7$, sodium rhenanite $CaNaPO_4$, and potassium rhenanite $CaKPO_4$. [9]. A necessary element of any strategy for improving the solubility of a compound with an ionic nature of the chemical bond is lowering the energy of the crystal lattice. Consistent implementation of this approach leads to two directions of increasing the resorption of calcium phosphate materials, as follows: (a) transition to calcium phosphates with a Ca/P ratio lower than that of HAP; (b) modification of the chemical composition associated with the replacement of the Ca^{2+} cation in the phosphate structure. Thus, ceramic materials based on CPP $Ca_2P_2O_7$ and rhenanite $CaMPO_4$, where (M = Na or K) are of great interest for different biomedical applications [10]. Ceramics based on CPP $Ca_2P_2O_7$ can be obtained in various ways during firing: (1) via heterophase reaction in powder mixture or condensed systems of crystals (such as cements) with Ca/P = 1 [11–13], (2) using thermal decomposition of hydrated calcium phosphates with Ca/P = 1 prepared for example via synthesis from solutions [14,15] or under conditions of mechanical activation [16]. Depending on the annealing temperature, various polymorphic modifications of $Ca_2P_2O_7$ can be obtained from hydrated calcium phosphates such as brushite or monetite: amorphous calcium pyrophosphate at 450 °C; γ-$Ca_2P_2O_7$–at 530 °C, β-$Ca_2P_2O_7$ at 700–750 °C, and α-$Ca_2P_2O_7$ at 1140–1179 °C [17].

Thus, to obtain ceramics containing a phase of CPP, it is necessary to use calcium phosphate powders with a ratio of Ca/P = 1. Brushite $CaHPO_4 \cdot 2H_2O$ (dicalcium phosphate dihydrate—DCPD) and monetite (dicalcium phosphate anhydrate—DCPA) can serve as a precursor for production of the ceramic materials based on CPP according to Equation (1).

$Ca_2P_2O_7$ can be obtained by thermal decomposition of brushite $CaHPO_4 \cdot 2H_2O$ powder, which is decomposed by rapid entry into an oven at 600 °C for 15 min [14]:

$$2CaHPO_4 \cdot 2H_2O \rightarrow Ca_2P_2O_7 + 3H_2O \tag{1}$$
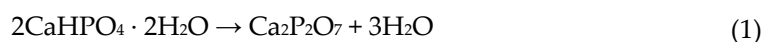
Monetite $CaHPO_4$ may be present in the brushite powder as an impurity phase, since it passes into calcium pyrophosphate during heat treatment (Equation (2)) [14]:

$$2CaHPO_4 \rightarrow Ca_2P_2O_7 + H_2O \tag{2}$$

Samples of brushite or monetite cement stone can also be used as precursors for the obtaining of ceramics based on calcium pyrophosphate. Brushite or monetite cement stone can be obtained as a result of chemical bonding reactions [5,11–13]. Brushite cements with the possibility of varying porosity and strength, high processability, can be produced according Equation (3) [18]:

$$Ca_3(PO_4)_2 + Ca(H_2PO_4)_2 \cdot H_2O + 7H_2O \rightarrow 4CaHPO_4 \cdot 2H_2O \tag{3}$$
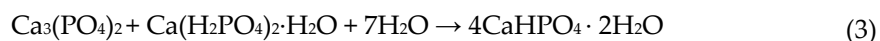
Monetite cements can be produced according Equation (4) [14]:

$$Ca_3(PO_4)_2 + Ca(H_2PO_4)_2 \cdot H_2O \rightarrow 4CaHPO_4 + H_2O \tag{4}$$

Brushite and monetite cements are used to close small defects in damaged teeth or bone tissues in the form of pastes or blocks of complex shape obtained from cement stone. The possibility of obtaining blocks of complex shape using cement technology, and the possibility of forming additional resorbable phases (CPP) during the firing of cement blocks allow us to consider brushite cements as the precursors for the production of ceramic materials [5,11,19].

A known method for producing rhenanite $CaNaPO_4$, is the crystallization of glass in the system SiO_2-Al_2O_3-Na_2O-K_2O-P_2O_5-F [20], or in SiO_2-CaO-Na_2O-P_2O_5-F-K_2O [21]. However, this method does not allow us to obtain rhenanite $CaNaPO_4$ as the only phase.

There is a method of processing phosphate ores using sodium carbonate or potassium chloride at temperatures of 300–900 °C, when the formation of sodium rhenanite $CaNaPO_4$ occurs only when the phosphate stone interacts with sodium carbonate [22]. This method is not suitable for the synthesis of sodium rhenanite $CaNaPO_4$ for medical uses.

It is well-known that sodium rhenanite $CaNaPO_4$ powder can be synthesized by heating a mixture of Na_2CO_3 and $Ca_2P_2O_7$ at 1000 °C for 10 h [23]. The solid-phase synthesis of sodium rhenanite $CaNaPO_4$ carried out in this way, is typical of any solid-phase synthesis, giving a powder with low sintering activity which will require higher temperatures to form ceramics based on it [9,10].

The ref. [24] shows a method for obtaining a material based on sodium rhenanite $CaNaPO_4$ from a charge containing sodium salt (sodium bicarbonate $NaHCO_3$) and calcium phosphate (monetite $CaHPO_4$). This process includes pressing the initial charge of powder mixture and firing at 1300 °C for 16 h. The main disadvantages of this method are the high temperature of the reaction and duration of the synthesis.

Rhenanites are very widely used to obtain phosphate fertilizers. Here, the ''Rhenania process'' should be mentioned, which is a well-known procedure used in the fertilizer industry to obtain soluble phosphate materials [25]. In this process, the natural mineral fluorapatite $Ca_5(PO_4)_3F$ is mixed with soda Na_2CO_3 and silicon dioxide SiO_2 while the molar ratio of Na_2CO_3/P_2O_5 is fixed at 1.0 (Equation (5)). The SiO_2 is added to prevent the occurrence of free CaO in the sintered product. These powder mixtures are crushed and then calcined in a rotary kiln at around 1000–1200 °C for several hours. Sodium rhenanite, a soluble $CaNaPO_4$, is the major phase in the final product of the Rhenania process.

$$Ca_5(PO_4)_3F + 2Na_2CO_3 + SiO_2 = 3CaNaPO_4 + Ca_2SiO_4 + 2CO_2\uparrow + NaF \qquad (5)$$

Furthermore, $CaNaPO_4$ can also be obtained via firing a mixture of CaO, H_3PO_4, and Na_2CO_3 at 1100 °C. Other starting components can be used for sodium rhenanite $CaNaPO_4$ preparation (Equation (6)):

$$2CaCO_3 + Na_2CO_3 + 2(NH_4)_2HPO_4 \rightarrow 2CaNaPO_4 + 3CO_2\uparrow + 4NH_3\uparrow + 3H_2O \ (t \sim 900\ °C) \qquad (6)$$

Alternatively, sodium rhenanite $CaNaPO_4$ can be obtained by cement technology with subsequent firing [26]. The work [27] shows a method for obtaining $CaNaPO_4$ from brushite cement, prepared by the reaction of β-TCP and, MCPM (Equation (3)), and a highly alkaline bioactive glass (composition (wt.%): $SiO_2 - 50$, $Na_2O - 25$, $CaO - 20$, $P_2O_5 - 5$). After mixing brushite with bioactive glass, firing was carried out at high temperatures. With an increase in the temperature to 700–800 degrees, $CaNaPO_4$, and $β-Ca_3(PO_4)_2$ phases were obtained, which indicates that the transition of bioactive glass to a visco-plastic state has occurred. The formation of the $CaNaPO_4$ phase occurs due to thermo-chemical interactions between Na_2O and CaO from the glass matrix and $β-Ca_2P_2O_7$.

Up to our knowledge there were attempts to prepare ceramic composites simultaneously containing both sodium rhenanite and calcium phosphate phases [23,28–30]. In some examples it was composition of sodium rhenanite with the calcium phosphate i.e with hydroxyapatite [28] or tricalcium phosphate [29]. In another example ceramics was prepared from powder of brushite, containing sodium nitrate as a reaction by-product [30].

The idea of this study is as follows—it is to obtain ceramics of a given phase composition by firing a cement-salt stone, which are easy to mold using plastic molding or extrusion 3D printing.

Therefore, the present work was aimed at obtaining bioresorbable ceramic materials in $Na_2O-CaO-P_2O_5$ system by firing a cement-salt stone obtained from powder mixtures including calcium citrate tetrahydrate $Ca_3(C_6H_5O_7)_2 \cdot 4H_2O$, MCPM $Ca(H_2PO_4)_2 \cdot H_2O$ and/or sodium dihydrogen phosphate NaH_2PO_4. We expected that the influence of the composition of starting powder mixture and firing temperature and on the phase composition and microstructure of ceramics would be established.
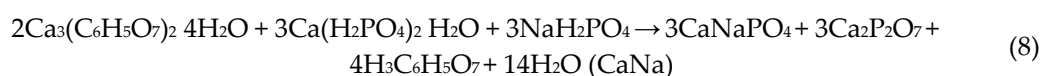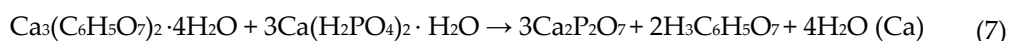
2. Materials and Methods

2.1. Initial Reagents and Synthesis

Calcium citrate tetrahydrate $Ca_3(C_6H_5O_7)_2 \cdot 4H_2O$ (CAS No. 5785-44-4, puriss. p.a. ≥85%), MCPM $Ca(H_2PO_4)_2 \cdot H_2O$ (CAS No. 10031-30-8, puriss. 99%) and sodium dihydrogen phosphate NaH_2PO_4 (CAS No. 7558-80-7, puriss. ≥ 99%) used for synthesis of cement-salt stone samples were purchased from Sigma Aldrich, (Taufkirchen, Germany).

2.2. Preparation of the Calcium Pyrophosphate and Sodium Rhenanite Ceramics

The following Equations (7)–(9) were used to calculate the composition of the powder mixtures for preparation of cement-salt stone samples. Labeling of samples are shown in brackets and in Table 1.

$$Ca_3(C_6H_5O_7)_2 \cdot 4H_2O + 3Ca(H_2PO_4)_2 \cdot H_2O \rightarrow 3Ca_2P_2O_7 + 2H_3C_6H_5O_7 + 4H_2O \text{ (Ca)} \quad (7)$$

$$2Ca_3(C_6H_5O_7)_2\ 4H_2O + 3Ca(H_2PO_4)_2\ H_2O + 3NaH_2PO_4 \rightarrow 3CaNaPO_4 + 3Ca_2P_2O_7 + \\ 4H_3C_6H_5O_7 + 14H_2O \text{ (CaNa)} \quad (8)$$

$$Ca_3(C_6H_5O_7)_2\ 4H_2O + 3NaH_2PO_4 \rightarrow 3CaNaPO_4 + 2H_3C_6H_5O_7 + 4H_2O \text{ (Na)} \quad (9)$$

Each component was previously treated in a planetary mill in an acetone medium for 15 min. Then initial mixtures, consisting of powders of calcium citrate tetrahydrate $Ca_3(C_6H_5O_7)_2 \cdot 4H_2O$, MCPM $Ca(H_2PO_4)_2 \cdot H_2O$ and/or sodium dihydrogen phosphate NaH_2PO_4 (Table 1), were prepared in a molar ratio corresponding to Equations (7)–(9) passing through a sieve several times. Mixing liquid (distilled water) were added to the resulting powder mixtures at a water/solid ratio (W/S) = 0.5. The resulting pastes were mixed in a porcelain bowl for 30 s. The latex mold with sizes of 10 × 10 × 30 mm was filled with prepared paste and left to harden in air for a day. The cement-salt stone samples after drying were fired in the temperature range of 500–900 °C with holding at the final temperature for 2 h, heating rate 5 °C/min, cooling with furnace.

Table 1. The expected phase composition of the ceramic materials and corresponding composition of the powder mixtures.

Symbol at Graph	Labeling	Molar ratio Na/Ca/P	The Composition of the Powder Mixture, g			Expected Phase Composition of Ceramics
			$Ca_3(C_6H_5O_7)_2 \cdot 4H_2O$ (g)	$Ca(H_2PO_4)_2 \cdot H_2O$ (g)	NaH_2PO_4 (g)	
a	Ca	0/1/1	43	57	0	β-$Ca_2P_2O_7$
b	CaNa	0.5/0.5/1	50,6	33,5	15,9	β-$Ca_2P_2O_7$ + β-$CaNaPO_4$
c	Na	1/1/1	61,3	0	38,7	β-$CaNaPO_4$

2.3. Characterization

2.3.1. XRD

X-ray diffraction (XRD) analysis was conducted using a Rigaku D/Max-2500 (Rigaku, Tokyo, Japan) with a rotating anode (Cu-Ka radiation), with an angle interval (2Θ) of 2–70°. Phase analysis was performed using the ICDD PDF2 database [31].

2.3.2. SEM

The microstructure of the samples of cement-salt and ceramic materials was studied using a LEO SUPRA 50VP (Carl Zeiss, Jena, Germany) scanning electron microscope (SEM) with an acceleration voltage of 3 – 21 kV. The images were recorded using an Everhart–Thornley secondary electron detector (SE2). The surface of the cement-salt stone and ceramic samples was coated with a layer of chromium (up to 15 nm).

2.3.3. Thermal analysis

Thermal analysis (TA) of cement-salt samples was carried out using a NETZSCH STA 409 PC Luxx thermal analyzer (NETZSCH, Selb, Germany), in the temperature range of 40–1000 °C. The composition of the gas phase formed upon decomposition of samples was studied using a QMS 403C Aёolos quadrupole mass spectrometer (NETZSCH, Selb, Germany) coupled to the NETZSCH STA 409 PC Luxx thermal analyzer. Mass spectra (MS) were recorded for $m/Z = 18$ (H_2O), as well as for $m/Z = 44$ (CO_2).

2.3.4. Determination of strength properties of the ceramic samples

The bending and compressive strengths of ceramic samples in form of balks were determined using universal testing machines LFV 10-T50 and P-05 (Walter + bai, Löhningen, Switzerland).

2.3.5. Determination of shrinkage and density of the ceramic samples

The shrinkage of ceramic samples was determined by measuring their dimensions (with an accuracy of ±0.05 mm) before and after firing. The geometric density of the ceramic samples was calculated by measuring their dimensions (with an accuracy of ±0.05 mm) and mass before and after firing. The relative density of ceramics was calculated as the ratio of the sample density determined from the experiment to the crystallographic density of β-$Ca_2P_2O_7$ and β-$CaNaPO_4$.
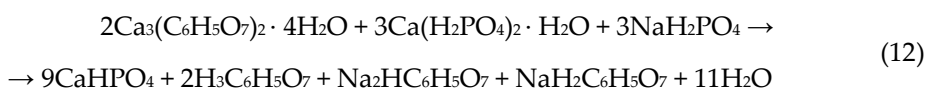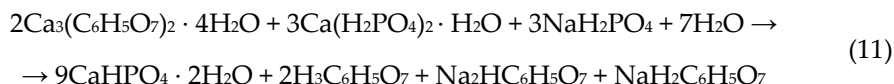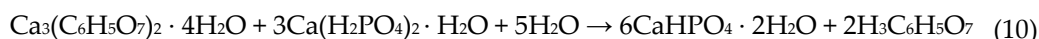
3. Results and Discussion

The XRD curves of the cement-salt stone based on calcium citrate tetrahydrate and MCPM (Ca); calcium citrate, tetrahydrate, MCPM and sodium dihydrogen phosphate (CaNa); and calcium citrate and sodium dihydrogen phosphate (Na) are shown in Figure 1.
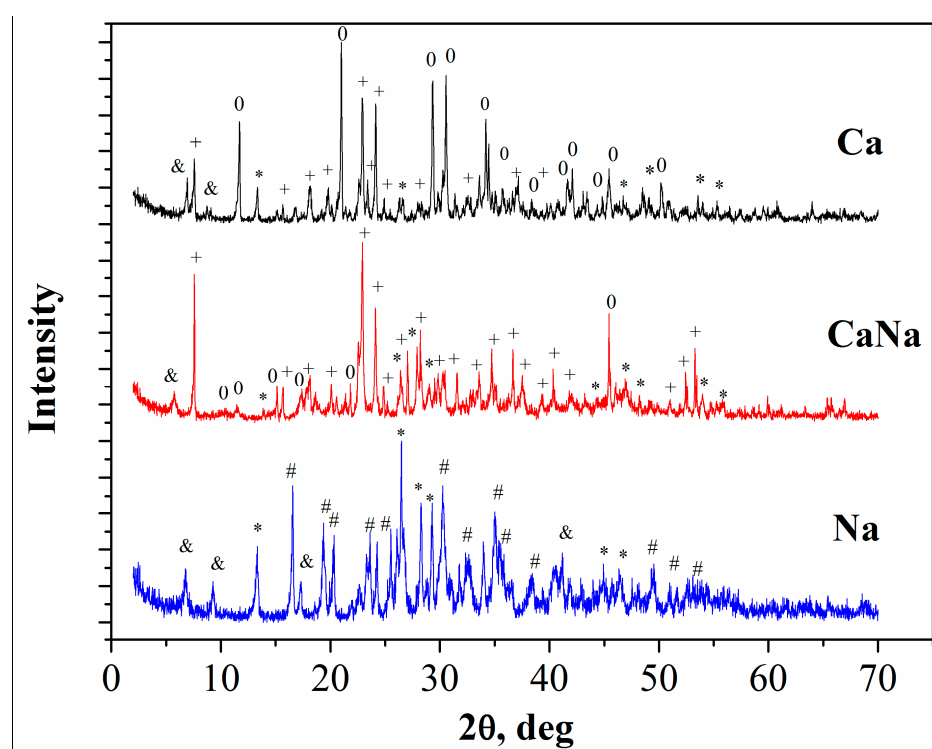
Figure 1. XRD spectra of the cement-salt stone: (**Ca – black curve**); (**CaNa – red curve**); (**Na – blue curve**). Symbols are as follows: 0—$CaHPO_4 \cdot 2H_2O$ (PDF 72-713); *—$CaHPO_4$ (PDF 75-1520); +—$Ca(H_2PO_4)_2 \cdot H_2O$ (PDF 9-347); &—$Ca_3(C_6H_5O_7)_2 \cdot 4H_2O$ (PDF 28-2003); #—NaH_2PO_4 (PDF 70-954).

The Equations (10)–(13) reflects the reaction of phase composition of cement-salt stone formation:

$$Ca_3(C_6H_5O_7)_2 \cdot 4H_2O + 3Ca(H_2PO_4)_2 \cdot H_2O + 5H_2O \rightarrow 6CaHPO_4 \cdot 2H_2O + 2H_3C_6H_5O_7 \quad (10)$$

$$2Ca_3(C_6H_5O_7)_2 \cdot 4H_2O + 3Ca(H_2PO_4)_2 \cdot H_2O + 3NaH_2PO_4 + 7H_2O \rightarrow$$
$$\rightarrow 9CaHPO_4 \cdot 2H_2O + 2H_3C_6H_5O_7 + Na_2HC_6H_5O_7 + NaH_2C_6H_5O_7 \quad (11)$$

$$2Ca_3(C_6H_5O_7)_2 \cdot 4H_2O + 3Ca(H_2PO_4)_2 \cdot H_2O + 3NaH_2PO_4 \rightarrow$$
$$\rightarrow 9CaHPO_4 + 2H_3C_6H_5O_7 + Na_2HC_6H_5O_7 + NaH_2C_6H_5O_7 + 11H_2O \quad (12)$$

$$Ca_3(C_6H_5O_7)_2 \cdot 4H_2O + 3NaH_2PO_4 \rightarrow 3CaHPO_4 + Na_2HC_6H_5O_7 + NaH_2C_6H_5O_7 + 4H_2O \quad (13)$$

According to the XRD data, the phase composition of cement-salt stone based on calcium citrate tetrahydrate $Ca_3(C_6H_5O_7)_2 \cdot 4H_2O$ and MCPM $Ca(H_2PO_4)_2 \cdot H_2O$ (Figure 1, Ca) was represented by brushite $CaHPO_4 \cdot 2H_2O$ and unreacted calcium citrate tetrahydrate $Ca_3(C_6H_5O_7)_2 \cdot 4H_2O$ and MCPM $Ca(H_2PO_4)_2 \cdot H_2O$ phases (Equation (10)) [5].

The main phases in the cement-salt stone based on calcium citrate tetrahydrate $Ca_3(C_6H_5O_7)_2 \cdot 4H_2O$ and sodium dihydrogen phosphate NaH_2PO_4 (Figure 1, Na) were monetite $CaHPO_4$, unreacted sodium dihydrogen phosphate NaH_2PO_4, and calcium citrate tetrahydrate $Ca_3(C_6H_5O_7)_2 \cdot 4H_2O$ (Equation (13)) [26].

The phase composition of the obtained samples of cement-salt stone based on calcium citrate tetrahydrate $Ca_3(C_6H_5O_7)_2 \cdot 4H_2O$, MCPM $Ca(H_2PO_4)_2 \cdot H_2O$ and sodium dihydrogen phosphate NaH_2PO_4 (Figure 1, CaNa) was included by brushite $CaHPO_4 \cdot 2H_2O$, monetite $CaHPO_4$, unreacted calcium citrate tetrahydrate $Ca_3(C_6H_5O_7)_2 \cdot 4H_2O$, MCPM $Ca(H_2PO_4)_2 \cdot H_2O$ and sodium dihydrogen phosphate NaH_2PO_4.

The formation of brushite $CaHPO_4 \cdot 2H_2O$ and monetite $CaHPO_4$ occurred as a result of acid-base interaction (Equations (10) - (13). Sodium dihydrogen phosphate NaH_2PO_4 (85.2 g/L) has a higher solubility than MCPM $Ca(H_2PO_4)_2 \cdot H_2O$ (18 g/L) and, accordingly, the concentration of hydrogen ions H^+ is higher (lower pH) in the CaNa sample and even more in the Na sample than in the Ca sample. This pH level makes the formation of monetite $CaHPO_4$ more likely [32].

The presence of unreacted components shows that the reaction has not been fully completed in the conditions given here. For Na and CaNa samples there are also peaks that probably correspond to the acidic calcium citrate salts, such as $Na_2HC_6H_5O_7$ and $NaH_2C_6H_5O_7$. We also assume that $Na_2HC_6H_5O_7$ and $NaH_2C_6H_5O_7$ phases of acidic sodium citrate are present in the preceramic sample, since they are by-products of the brushite formation reaction, which is exactly present in the X-ray pattern presented in Figure 1.

The microstructure studies of the cement-salt stone support the results of the XRD data. The micrographs of the samples demonstrated in Figure 2 show small crystals of monetite $CaHPO_4$ and brushite $CaHPO_4 \cdot 2H_2O$ with plate-like morphology [33–35], rhombic crystals of MCPM $Ca(H_2PO_4)_2 \cdot H_2O$ [36,37]. The $CaHPO_4 \cdot 2H_2O$ and $CaHPO_4$ crystals are most likely formed on the surface of the less soluble among other starting components of powder mixture calcium citrate particles. The $CaHPO_4$ crystals have a size of less than 2 μm probably due to the action of $C_6H_5O_7^{3-}$ anion which slows down the reaction and inhibits the growth of calcium hydrogen phosphate crystals [38].
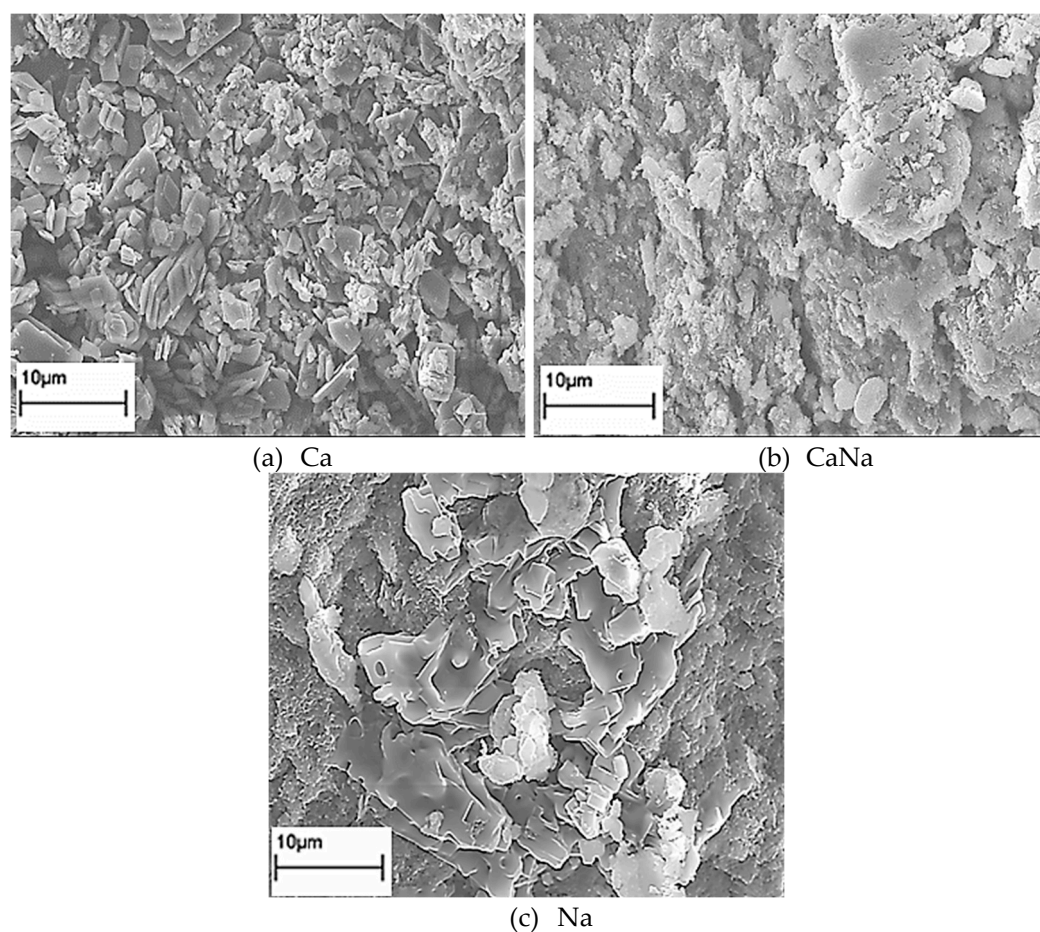
**Figure 2.** The SEM images of cement-salt stone: Ca (**a**), CaNa (**b**); Na (**c**).

The following TA data of the obtained samples are shown in Figure 3: the temperature dependence of the mass of samples of cement-salt stone based on calcium citrate tetrahydrate and MCPM (Ca, Figure 3a,b); calcium citrate tetrahydrate and sodium dihydrogen phosphate (Na, Figure 3a,c); calcium citrate tetrahydrate, MCPM and sodium dihydrogen phosphate (CaNa, Figure 3a,d), the temperature dependence of the ion current for all samples for $m/Z = 18$ (H_2O) (Figure 3e), and $m/Z = 44$ (CO_2) (Figure 3f).

(c) Na   (d) CaNa

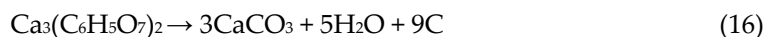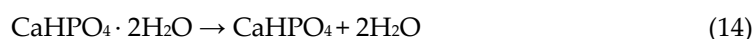(e) MS (m/Z=18)   (f) MS (m/Z=44)
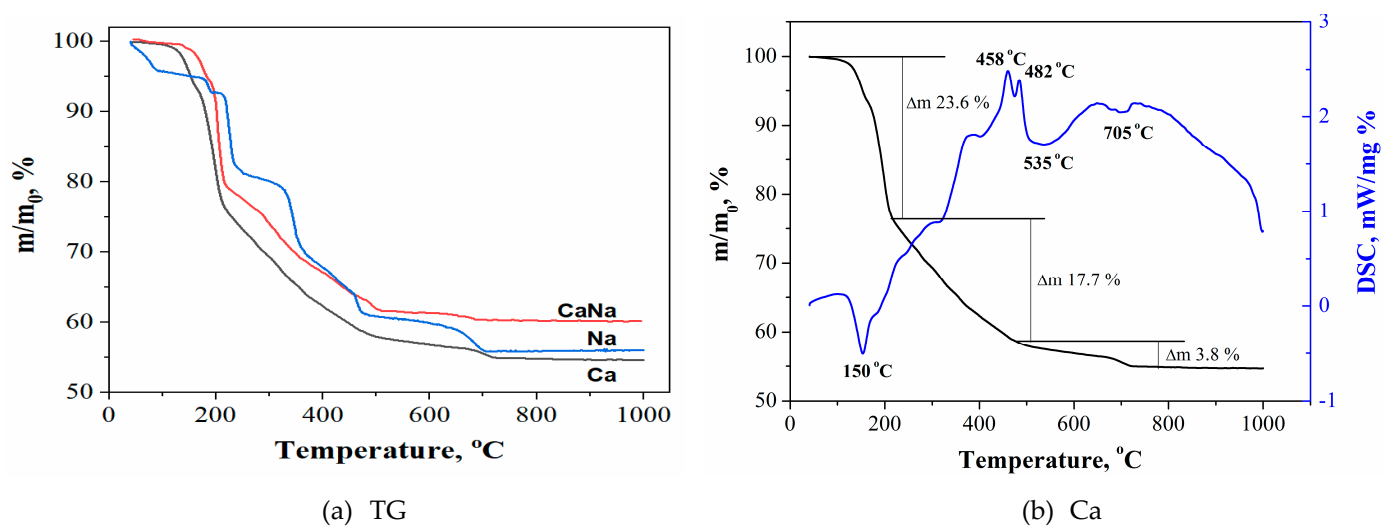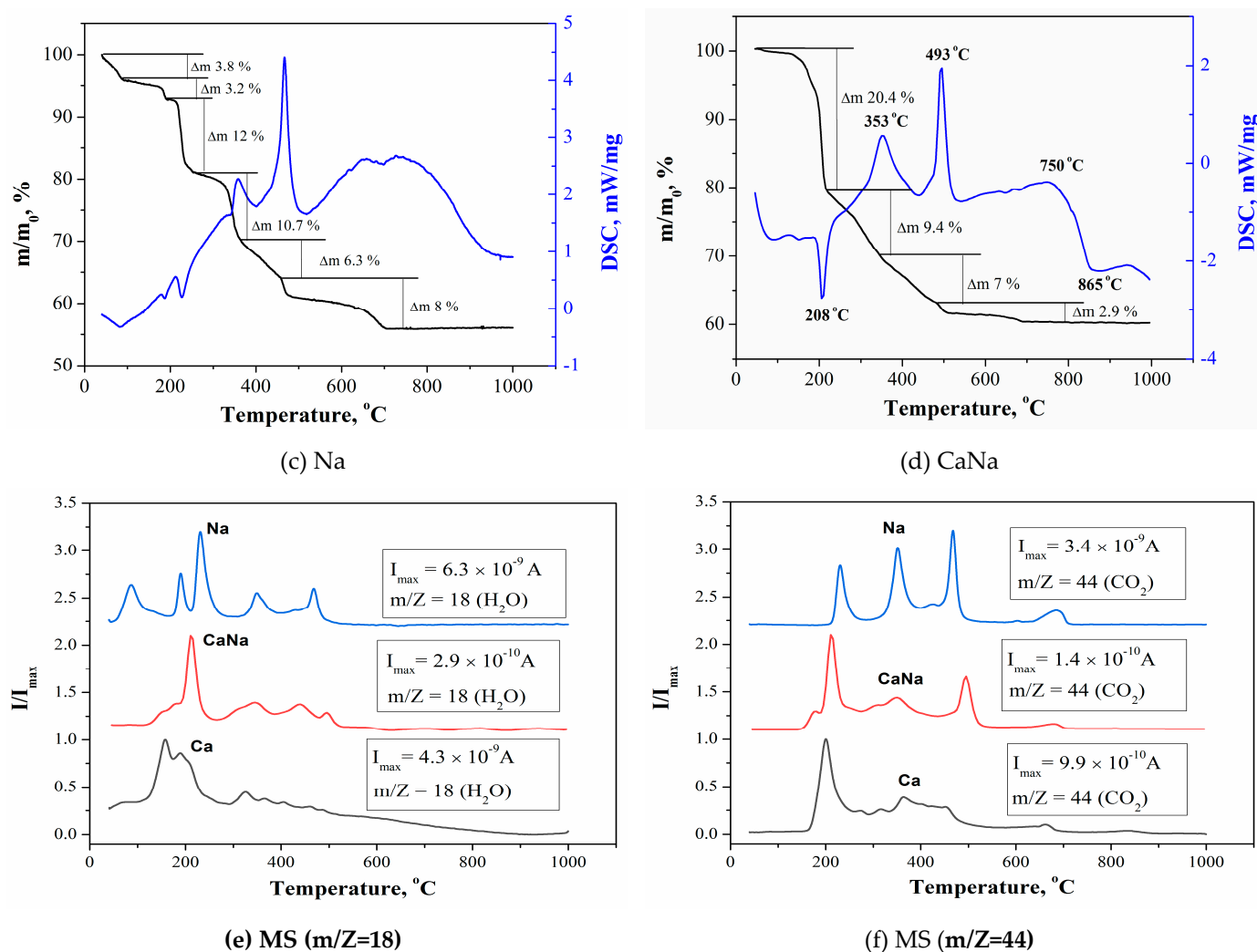
Figure 3. Thermal analysis of the cement-salt stone: (a) TG; (b) TG/DTA curves obtained for the Ca synthesized powders; (c) TG/DTA curves obtained for the Na synthesized powders; (d) TG/DTA curves obtained for the CaNa synthesized powders; (e, f) ion current curves according to mass spectroscopy for m/Z = 18 (H_2O) (e) and for m/Z = 44 (CO_2) (f), respectively.
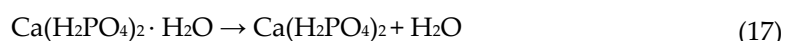
According to simultaneous thermal analysis (Figure 3a,b), the total weight loss of the powder mixture based on calcium citrate and MCPM when heated to 1000 °C was 46%. The mass loss curve for Ca powder mixture (Figure 3a,b) contains steps characteristic of brushite, namely, the conversion of brushite to monetite (~200 °C, equation 14), and then monetite to pyrophosphate (~400 °C, equation 15). There are two endothermic peaks on the DSC curve in the first temperature range (150°C, and 190°C). Three peaks can be observed on the mass spectrum curve for m/Z = 18 (H_2O) in the range of 150–300 °C at the same temperatures (Figure 3e). In this temperature range, thermal decomposition of calcium citrate tetrahydrate $Ca_3(C_6H_5O_7)_2 \cdot 4H_2O$ and brushite $CaHPO_4 \cdot 2H_2O$ with the formation of anhydrous calcium citrate $Ca_3(C_6H_5O_7)_2$ and monetite $CaHPO_4$ is possible. On the mass spectrum curve for m/Z = 44 in the range of 370-480 °C, reflecting the release of CO_2. Thermal decomposition of anhydrous calcium citrate $Ca_3(C_6H_5O_7)_2$ with the formation of calcium carbonate $CaCO_3$ occurs with heat release (DSC curve) according to the equation 16. The carbon resulting from this transformation (reaction) could not naturally remain in elemental form at such a high temperature (above 340°C), especially in the presence of atmospheric oxygen. Therefore, it must have turned into CO and/or CO_2.

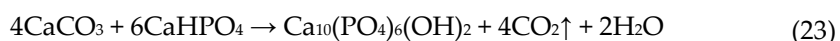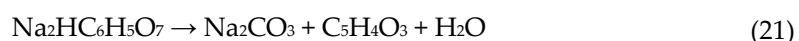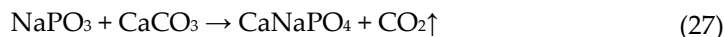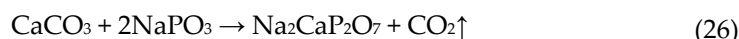We can suggest the following reactions that can take place during heating:

$$CaHPO_4 \cdot 2H_2O \rightarrow CaHPO_4 + 2H_2O \tag{14}$$

$$2CaHPO_4 \rightarrow Ca_2P_2O_7 + H_2O \tag{15}$$

$$Ca_3(C_6H_5O_7)_2 \rightarrow 3CaCO_3 + 5H_2O + 9C \tag{16}$$

In the temperature range of 480-705 °C, the following processes is observed: MCPM $Ca(H_2PO_4)_2 \cdot H_2O$ present in the samples also undergoes a series of transformations, forming calcium polyphosphate $Ca(PO_3)_2$ (equations (17)-(19)). Also, β-CPP β-$Ca_2P_2O_7$ phase was formed due to the interaction of calcium polyphosphate $Ca(PO_3)_2$ with calcium carbonate $CaCO_3$ (equations (20)):

$$Ca(H_2PO_4)_2 \cdot H_2O \rightarrow Ca(H_2PO_4)_2 + H_2O \tag{17}$$

$$Ca(H_2PO_4)_2 \rightarrow CaH_2P_2O_7 + H_2O \tag{18}$$

$$CaH_2P_2O_7 \rightarrow Ca(PO_3)_2 + H_2O \tag{19}$$

$$Ca(PO_3)_2 + CaCO_3 \rightarrow Ca_2P_2O_7 + CO_2\uparrow \tag{20}$$

The presence of unreacted starting components in the samples and the by-products of chemical bonding reaction determine the presence of additional steps of mass loss and peaks on the curves of the dependence of the ion current on temperature (Figure 3e, f) [5].

According to the TG data, the final mass loss of the Na powder after heating to 1000 °C was 44 % (Figure 3a,c). At the first stage (up to 160 °C), there was a gradual decomposition of structurally unbonded water. At the next stage (up to 200 °C), the transition of brushite to monetite took place, but according to TA, the content of brushite was not significant. The further process is the transformation of monetite to γ -pyrophosphate γ-CPP (equation (15)), generally takes place at 400 °C [5,11–13,16]. According to mass spectroscopy for cement-salt stone based on powder mixture of calcium citrate tetrahydrate $Ca_3(C_6H_5O_7)_2 \cdot 4H_2O$ and sodium dihydrogen phosphate NaH_2PO_4 (Figure 3b) three peaks can be observed on the mass spectrum curve for m/Z = 18 (H_2O) in the range of 50–300 °C. In this temperature range, thermal decomposition of calcium citrate tetrahydrate $Ca_3(C_6H_5O_7)_2 \cdot 4H_2O$ with the formation of anhydrous calcium citrate $Ca_3(C_6H_5O_7)_2$ is possible. On the mass spectrum curve for m/Z = 44, there is a peak in the range of 435–495 °C, reflecting the release of CO_2. Thermal decomposition of anhydrous calcium citrate $Ca_3(C_6H_5O_7)_2$ with the formation of calcium carbonate $CaCO_3$ occurs with heat release according to the equation (16) [26]. On the mass spectrum curve for m/Z = 44 in the range of 650-705 °C, reflecting the release of CO_2. The formation of the $CaNaPO_4$ phase was due to the interaction of the $NaPO_3$ melt with calcium carbonate $CaCO_3$ (equation (27)) can be the reason of this CO_2 release. During the heat treatment, the products obtained during the acid-base reaction thermally decomposed, and products of thermal decomposition interacted with each other to form ceramics. The processes taking place during heating can be described by the following equations:

$$Na_2HC_6H_5O_7 \rightarrow Na_2CO_3 + C_5H_4O_3 + H_2O \tag{21}$$

$$NaH_2PO_4 \rightarrow NaPO_3 + H_2O \tag{22}$$

$$4CaCO_3 + 6CaHPO_4 \rightarrow Ca_{10}(PO_4)_6(OH)_2 + 4CO_2\uparrow + 2H_2O \tag{23}$$

$$Ca_{10}(PO_4)_6(OH)_2 + NaPO_3 \rightarrow CaNaPO_4 + 3Ca_3(PO_4)_2 + H_2O \tag{24}$$

$$Na_2CO_3 + Ca_2P_2O_7 \rightarrow 2CaNaPO_4 + CO_2\uparrow \tag{25}$$

$$CaCO_3 + 2NaPO_3 \rightarrow Na_2CaP_2O_7 + CO_2\uparrow \tag{26}$$

$$NaPO_3 + CaCO_3 \rightarrow CaNaPO_4 + CO_2\uparrow \tag{27}$$

$$Na_2CaP_2O_7 + Ca_{10}(PO_4)_6(OH)_2 \rightarrow Ca_{10}Na(PO_4)_7 + CaNaPO_4 + H_2O \tag{28}$$

According to the TG data, the final mass loss of the CaNa powder after heating to 1000 °C was 40 % (Figure 3a,d). Three peaks can be observed on the mass spectrum curve for m/Z = 18 (H_2O) in the range of 200–400 °C. In this temperature range, thermal decomposition of calcium citrate tetrahydrate $Ca_3(C_6H_5O_7)_2 \cdot 4H_2O$ with the formation of anhydrous calcium citrate $Ca_3(C_6H_5O_7)_2$ is possible. The mass loss curve for the sample based on calcium citrate tetrahydrate, monocalcium phosphate monohydrate, and sodium dihydrogen phosphate contains steps characteristic of brushite, namely the conversion of brushite to monetite (~200°C), and then the conversion of monetite to γ-CPP (~400 °C). The presence of unreacted starting components in the samples (a component taken in excess) and the accompanying reaction products determine the presence of additional steps of mass loss and peaks on the curves of the dependence of the ion current on temperature (Figure 3b). On the mass spectrum curve for m/Z = 44, there is a peak in the range of 200–495 °C, reflecting the release of CO_2. Thermal decomposition of anhydrous calcium citrate $Ca_3(C_6H_5O_7)_2$ with the formation of calcium carbonate $CaCO_3$ occurs with heat release according to the equation (16) [39].

The carbon formed as a result of this transformation (equation (16)) could not remain in elemental form at such a high temperature (above 340 °C), especially in the presence of atmospheric oxygen. Therefore, it must have turned into CO and/or CO_2. In the temperature range of 495–680 °C, the following process is observed: MCPM $Ca(H_2PO_4)_2 \cdot H_2O$ present in the samples also undergoes a series of transformations, forming calcium polyphosphate $Ca(PO_3)_2$ (equations (17)-(19)). Also, β-CPP β-$Ca_2P_2O_7$ phase was formed due to the interaction of calcium polyphosphate $Ca(PO_3)_2$ with calcium carbonate $CaCO_3$ (equations (20)).

After annealing of cement-salt stone Ca at 500 °C phase composition of the ceramic materials was represented by γ-$Ca_2P_2O_7$ and γ-$Ca(PO_3)_2$. In the temperature range of 700-900 °C γ-$Ca(PO_3)_2$ and γ-$Ca_2P_2O_7$ phases passed into a higher-temperature modifications (β-$Ca(PO_3)_2$ and β-$Ca_2P_2O_7$). And after firing at 900 °C phase composition included β-$Ca_2P_2O_7$ (Figure 4). And after annealing at 1000 °C the phase composition of ceramics was presented only with β-$Ca_2P_2O_7$ [5].

During the heat treatment of cement-salt stone Na at temperatures of 500 and 700 °C in addition to the target phase β-$CaNaPO_4$, hydroxyapatite $Ca_{10}(PO_4)_6(OH)_2$ was formed. At 700 °C, in addition to β-$CaNaPO_4$ and $Ca_{10}(PO_4)_6(OH)_2$, phases of double calcium-sodium pyrophosphate $CaNa_2P_2O_7$ and β-$Ca_3(PO_4)_2$ phases were formed [26]. At 900 °C, only the target phase β-$CaNaPO_4$ was found (Figure 4).

Heat treatment of cement-salt stone CaNa at a temperature of 500 °C (Figure 5) led to the formation of a phase composition, which included the β-$CaNaPO_4$, $Ca_{10}(PO_4)_6(OH)_2$, and γ-$Ca_2P_2O_7$ phases (equations (15) and (24)). The $Ca_{10}(PO_4)_6(OH)_2$ phase was formed due to the interaction of monetite $CaHPO_4$ with calcium carbonate $CaCO_3$ (equation (23)) which was the product of the calcium citrate $Ca_3(C_6H_5O_7)_2$ decomposition (equation (16)). After heat treatment at temperatures of 700 °C and 900 °C, in addition to β-$CaNaPO_4$, phases of β-$Ca_2P_2O_7$, double calcium-sodium pyrophosphate $Na_2CaP_2O_7$ and Na–substituted tricalcium phosphate $Ca_{10}Na(PO_4)_7$ phases were noticed. The formation of the $Na_2CaP_2O_7$ phase was due to the possible interaction of the $NaPO_3$ melt with calcium oxide $CaCO_3$ (equation (26)). The $Ca_{10}Na(PO_4)_7$ phase was formed as a result of the interaction of $Na_2CaP_2O_7$ with $Ca_{10}(PO_4)_6(OH)_2$ (equation (28)).
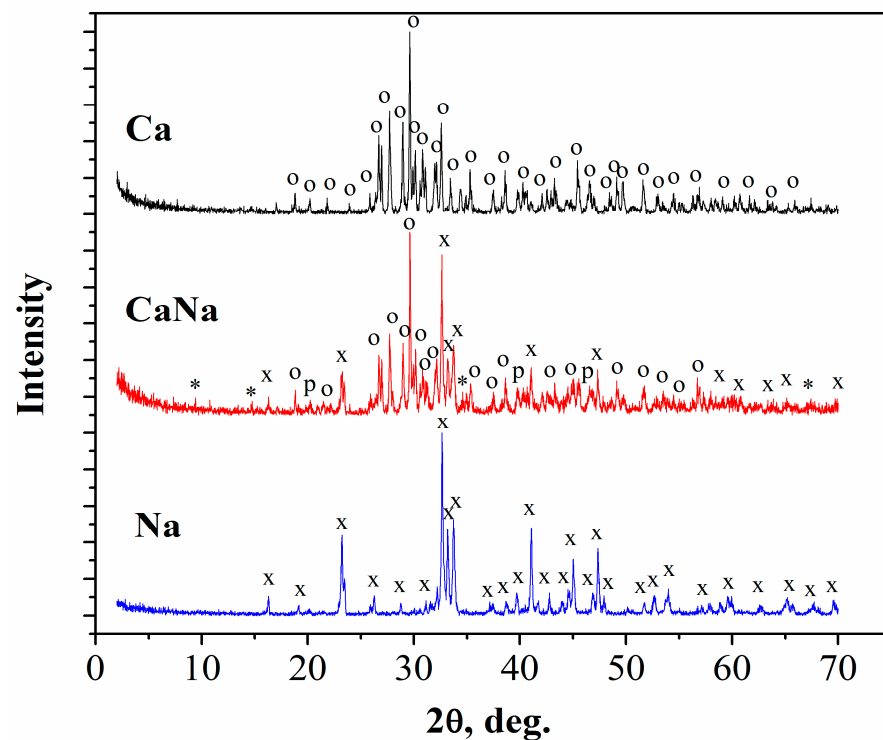
Figure 4. The XRD of ceramic samples based on cement-salt stone: Na (**black-curve**), CaNa (**red-curve**) and Ca (**blue-curve**) in the temperature of 900 °C. x—β-CaNaPO$_4$ (PDF 29-1193); p—Na$_2$CaP$_2$O$_7$ (PDF 48-557); o—β-Ca$_2$P$_2$O$_7$ (PDF 9-346); *—Ca$_{10}$Na(PO$_4$)$_7$ (PDF 45-339).
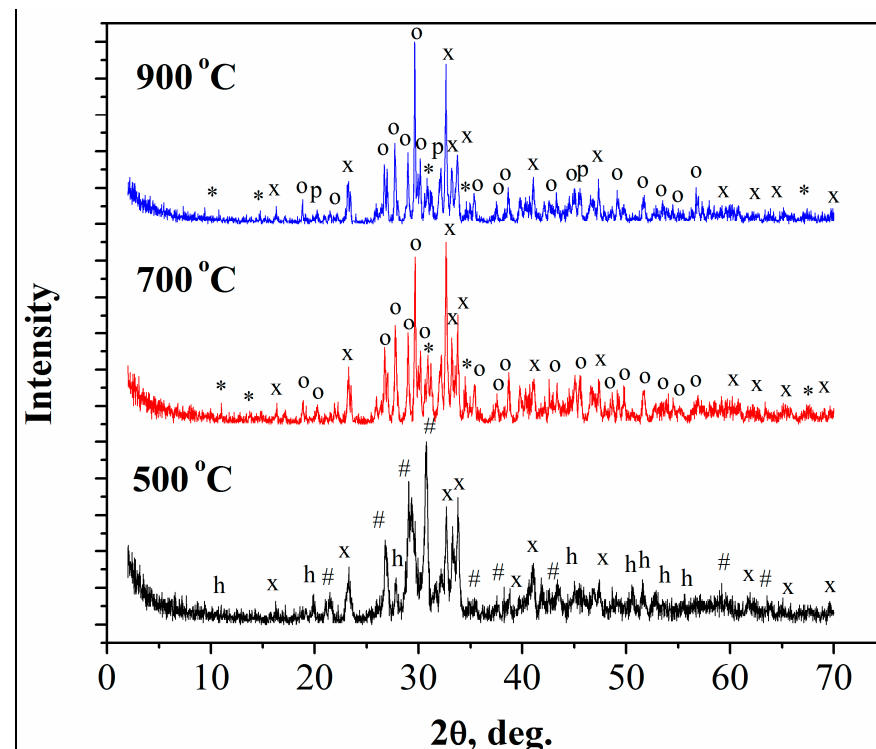

Figure 5. The XRD of ceramic samples based on cement-salt stone CaNa in the temperature range of 500-900 °C. h—Ca$_{10}$(PO$_4$)$_6$(OH)$_2$ (PDF 74-565), x—β-CaNaPO$_4$ (PDF 29-1193); #—Υ-Ca$_2$P$_2$O$_7$ (PDF 17-499); p—Na$_2$CaP$_2$O$_7$ (PDF 48-557); o—β-Ca$_2$P$_2$O$_7$ (PDF 9-346); *—Ca$_{10}$Na(PO$_4$)$_7$ (PDF 45-339).

The linear shrinkage of ceramic materials is shown in Figure 6. The linear shrinkage of the Ca samples was 2.5 % and 3.5 % at 500 °C and 900 °C, respectively. The density of

ceramics has decreased compared to the density of cement-salt stone. The decrease in the density of the samples was due to a decrease in the mass of the sample, because of the decomposition of the components of the cement-salt stone during heating (Figure 7). The density of Ca samples (Figure 7) increased from 0.52 g/cm³ to 0.59 g/cm³ with an increase in firing temperature from 500 °C to 900 °C or from 41.8 % to 60 % relatively to the density of β-Ca$_2$P$_2$O$_7$ equal to 3.09 g/cm³ (Figure 8) [5].

The linear shrinkage of the Na samples was 2.7 % and 18.5 % at 500 °C and 900 °C, respectively (Figure 6). With an increase in firing temperature from 500 °C to 900 °C, the density of Na samples increased from 0.56 g/cm³ to 0.94 g/cm³ or from 18 % to 30.2% relatively to the density of β-CaNaPO$_4$ equal to 3.11 g/cm³ [26].

The linear shrinkage of the CaNa samples was 4.4 % and 20.1 % at 500 °C and 900 °C, respectively (Figure 6). The density of CaNa samples increased from 0.9 g/cm³ to 1.43 g/cm³ or from 30.9 % to 49.1 % relatively to the theoretical density of the ceramic sample calculated additively from the proportion of the following phases β-Ca$_2$P$_2$O$_7$ (ϱ=3.09 g/cm³), β-CaNaPO$_4$ (ϱ=3.11 g/cm³), Na$_2$CaP$_2$O$_7$ (ϱ=2.24 g/cm³) and Ca$_{10}$Na(PO$_4$)$_7$ (ϱ=3.02 g/cm³).
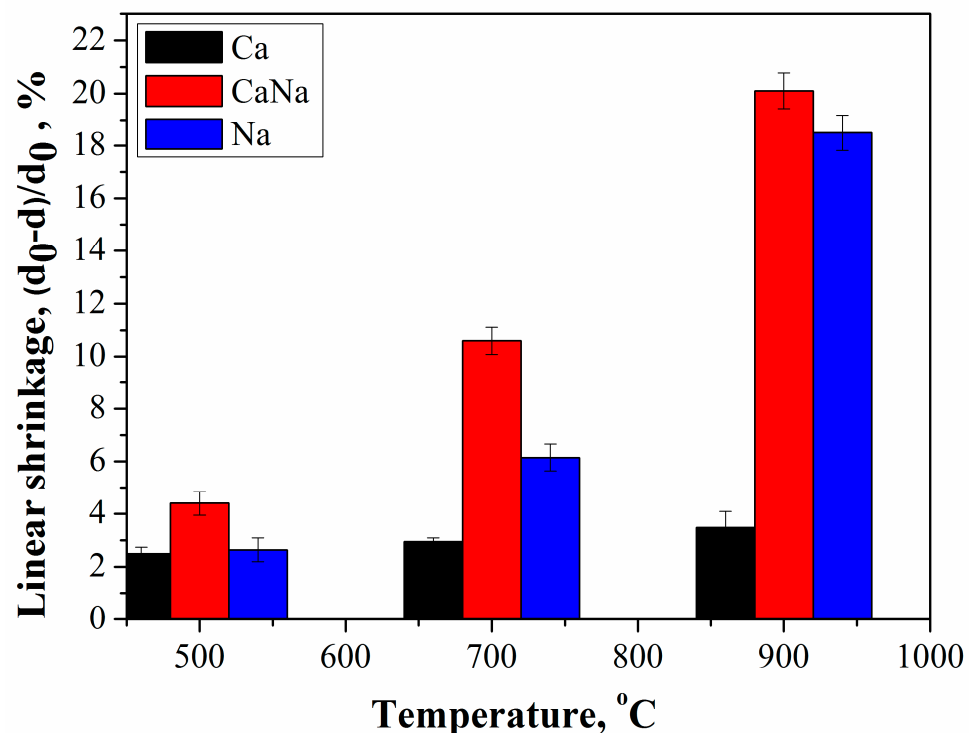
Figure 6. Linear shrinkage of ceramic samples obtained by annealing of cement-salt stone in the temperature range of 500–900 °C.
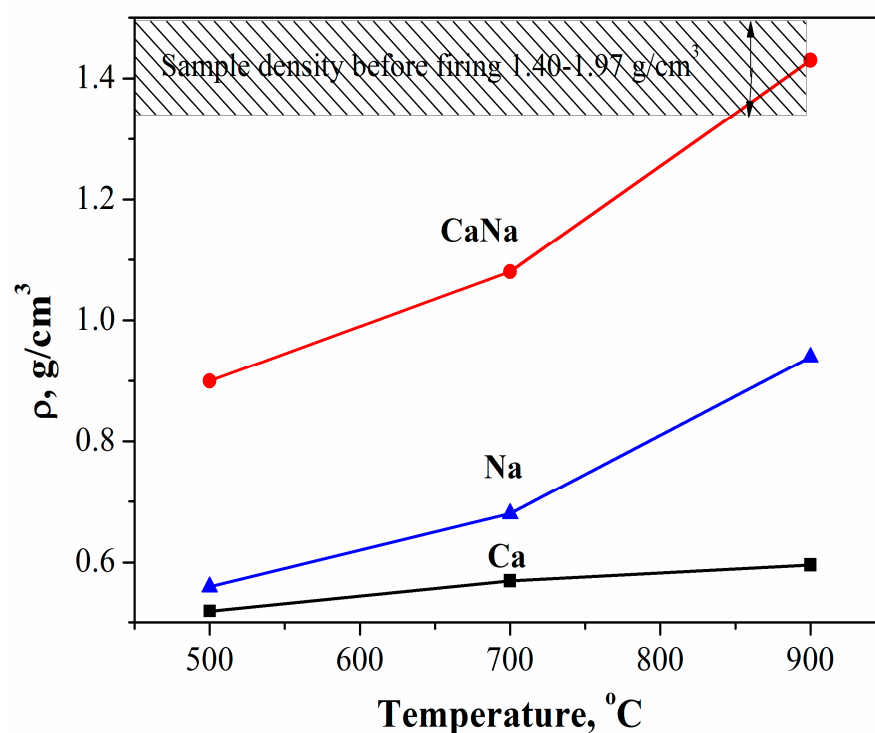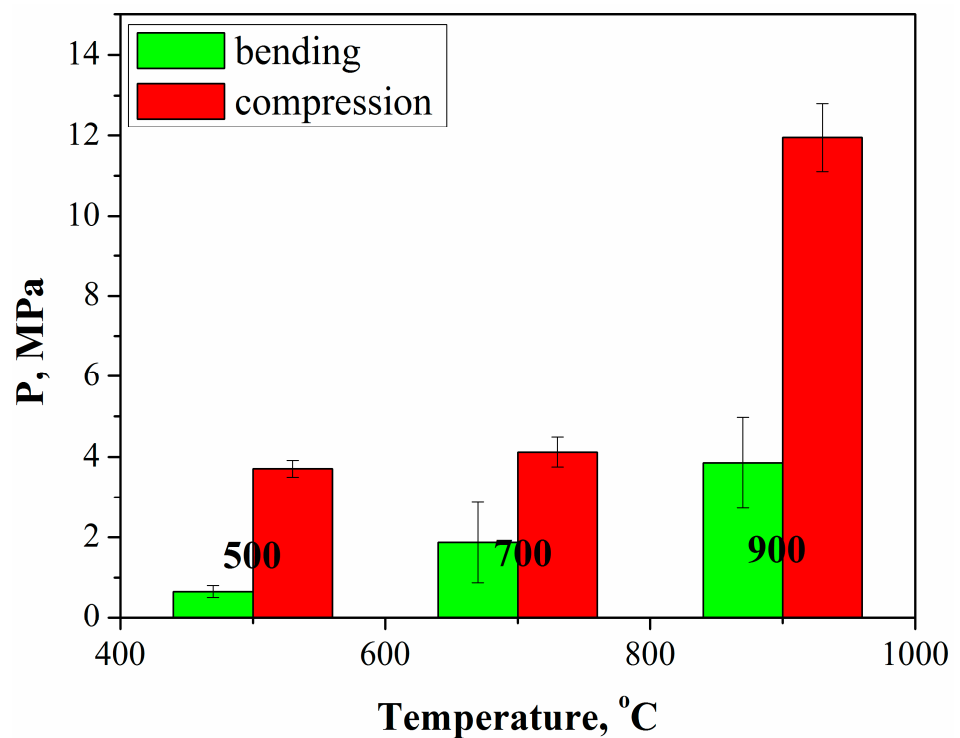
Figure 7. Density of ceramic materials, obtained by annealing of cement-salt stone in the temperature range of 500–900 °C.
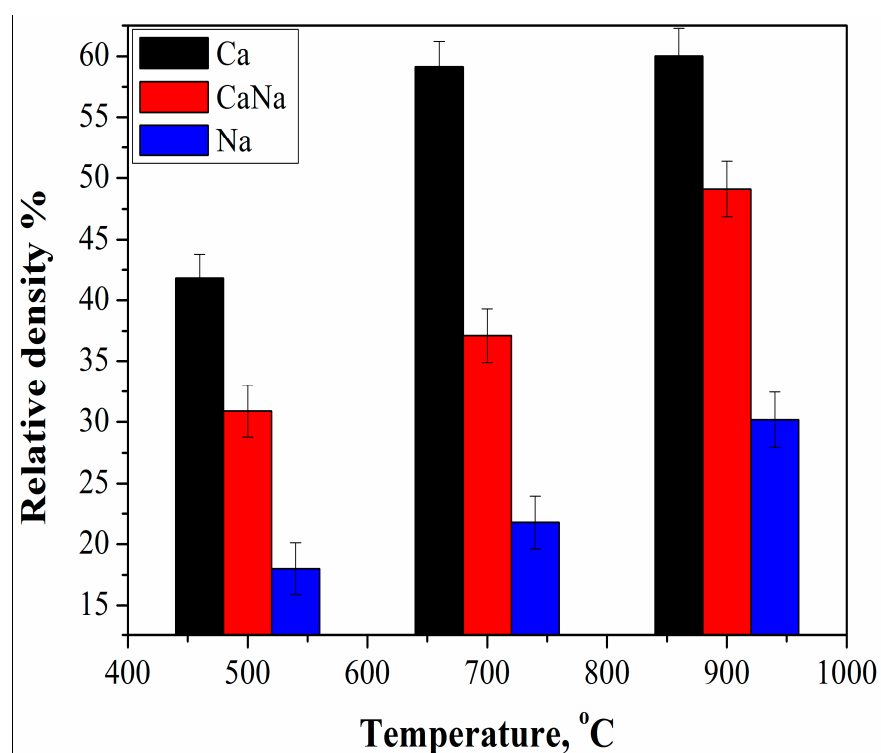
Figure 8. Relative density of ceramic samples, obtained via annealing of cement-salt stone in the temperature range of 500–900 °C.

Figure 9 shows the temperature dependence of compressive and bending strengths of CaNa ceramic materials.

Figure 9. The compressive and bending strengths of the CaNa ceramic samples after annealing at temperature range of 500–900 °C.

The compressive strength of Ca ceramic samples increased from 3.9 to 17.3 MPa and bending strength from 2.5 to 5.0 MPa increasing temperature from 600 °C to 1000 °C [5]. The compressive strength of Na ceramic samples increased from 3.5 to 10.3 MPa and bending strength from 2.5 to 3.6 MPa with increasing temperature from 500 °C to 900 °C [26]. The compressive strength of CaNa ceramic samples increase from 3.7 to 11.9 MPa and bending strength from 0.6 to 3.8 MPa with increasing temperature from 500 °C to 900 °C. This compressive and bending strength increasement is associated with the process of liquid-phase sintering, leading to the formation of more durable contacts between grains. The highest strength was in the Ca sample, the lowest is in the Na sample. Low strength is associated with a phase transition from β-CaNaPO$_4$ to α-CaNaPO$_4$. However, the strength of all samples is sufficient for surgical applications and for the treatment of bone tissue defects [40].

The SEM images of the Ca, CaNa, Na ceramic samples after firing at temperatures of 500 °C, 700 °C and 900 °C are shown in Figure 10.

(a) 500 °C   (b) 700 °C
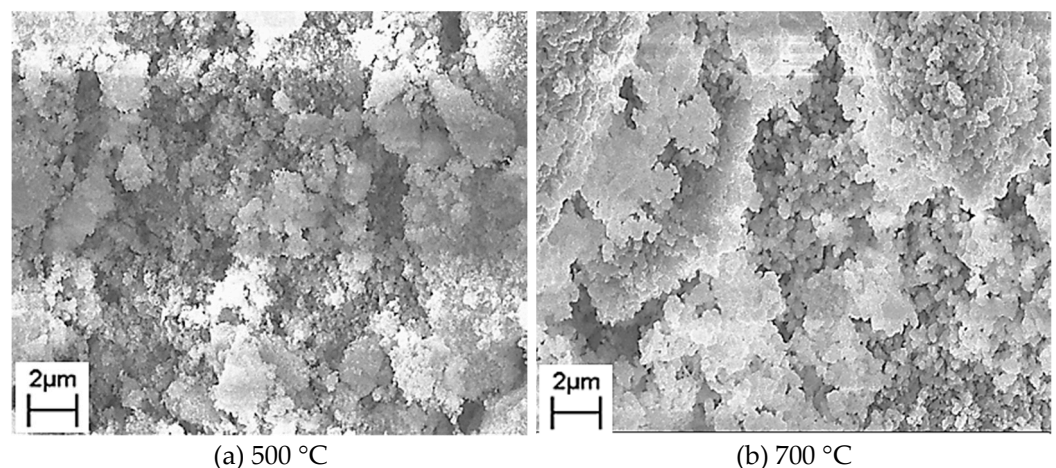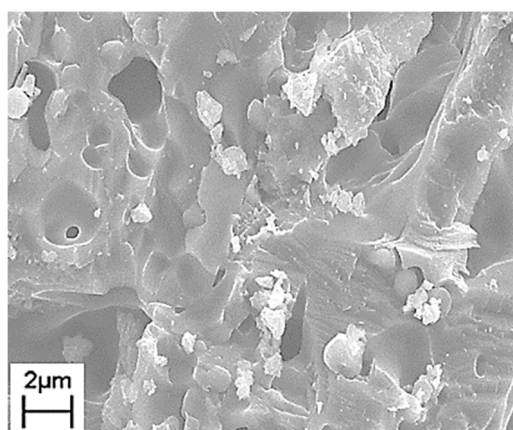
(c) 900 °C

Figure 10. The SEM images of ceramic CaNa samples based on cement-salt stone prepared from powder mixture of calcium citrate tetrahydrate, MCPM, and sodium dihydrogen phosphate, after firing at temperatures of 500 °C (**a**), 700 °C (**b**), and 900 °C (**c**).
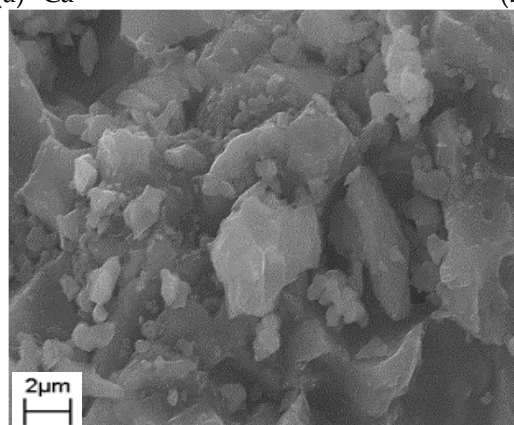
With an increase in the firing temperature, the grain size increases and the microstructure of ceramics changed. Spherical grains of 0.5-2 μm in size were found in a sample of CaNa ceramic material fired at a temperature of 500 °C. The spherical grains sintered, forming a porous microstructure. The microstructure of the ceramic material CaNa fired at 700 °C was represented by spherical grains with a size in the range 1-2 μm. The CaNa sample fired at 900 °C was distinguished by bigger crystals with a size in the range of 1-5 μm.

The microstructure of the obtained Ca, CaNa and Na ceramic samples after firing at 900 °C are shown in Figure 11.
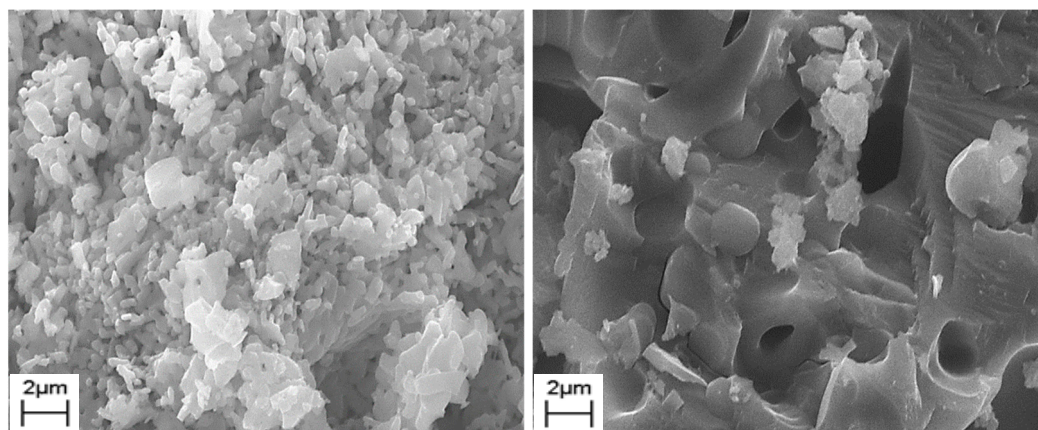
(a) Ca

(b) CaNa

(c) Na

Figure 11. The SEM images of ceramic samples based on cement-salt stone: Ca (**a**), CaNa (**b**), and Na (**c**), after firing at a temperature of 900 °C.

With an increase in the heat treatment temperature, the sintering of the samples proceeds more efficiently. The elimination of pores and the growth of grains take place. The grains size of Ca sample of ceramic was 1–2 μm when fired at 900 °C (Ca), while the grain sizes for the other samples was 1–3 μm (Na) and 1–5 μm (CaNa) when fired at 900 °C.

4. Conclusions

1. In the present work, an approach to obtaining bioresorbable ceramic materials in Na_2O-CaO-P_2O_5 system with a given phase composition, including β-CPP β-$Ca_2P_2O_7$, sodium rhenanite $CaNaPO_4$, double calcium-sodium pyrophosphate $Na_2CaP_2O_7$, and Na–substituted tricalcium phosphate $Ca_{10}Na(PO_4)_7$ was obtained by firing cement-salt stone from a powder mixture including calcium citrate tetrahydrate $Ca_3(C_6H_5O_7)_2 \cdot 4H_2O$, MCPM $Ca(H_2PO_4)_2 \cdot H_2O$ and sodium dihydrogen phosphate NaH_2PO_4. This approach involved the preparation of a powder mixtures with a given molar ratios of Na:Ca:P = 0:1:1(Ca), Na:Ca:P = 0,5:0,5:1(CaNa), Na:Ca:P = 1:1:1(Na), which were capable of entering into a chemical reaction; molding samples of cement-salt stone; and firing samples of cement-salt stone to obtain ceramics.

2. The phase composition of Ca and Na cement-salt stone samples was represented by brushite ($CaHPO_4 \cdot 2H_2O$), monetite ($CaHPO_4$) and unreacted $Ca_3(C_6H_5O_7)_2 \cdot 4H_2O$, $Ca(H_2PO_4)_2 \cdot H_2O$ and NaH_2PO_4 respectively. CaNa cement-salt stone samples were prepared from a powder mixture with a molar ratio of Na:Ca:P = 0,5:0,5:1, including calcium citrate tetrahydrate $Ca_3(C_6H_5O_7)_2 \cdot 4H_2O$, MCPM $Ca(H_2PO_4)_2 \cdot H_2O$ and sodium dihydrogen phosphate NaH_2PO_4. The phase composition of cement-salt stone samples based on $Ca_3(C_6H_5O_7)_2 \cdot 4H_2O$, $Ca(H_2PO_4)_2 \cdot H_2O$ and NaH_2PO_4 was represented mainly by brushite $CaHPO_4 \cdot 2H_2O$, monetite $CaHPO_4$, as well as unreacted $Ca(H_2PO_4)_2 \cdot H_2O$, NaH_2PO_4 and $Ca_3(C_6H_5O_7)_2 \cdot 4H_2O$.

3. After annealing of cement-salt stone Ca at 500 °C phase composition of the ceramic materials was represented by γ-$Ca_2P_2O_7$ and γ-$Ca(PO_3)_2$. In the temperature range of 700-900 °C γ-$Ca(PO_3)_2$ and γ-$Ca_2P_2O_7$ phases passed into a higher-temperature modifications (β-$Ca(PO_3)_2$ and β-$Ca_2P_2O_7$). And after annealing at 1000 °C the phase composition of ceramics was presented only with β-$Ca_2P_2O_7$.

   During the heat treatment of cement-salt stone Na at temperatures of 500 and 700 °C in addition to the target phase β-$CaNaPO_4$, hydroxyapatite $Ca_{10}(PO_4)_6(OH)_2$ was formed. At 700 °C, in addition to β-$CaNaPO_4$ and $Ca_{10}(PO_4)_6(OH)_2$, phases of double calcium-sodium pyrophosphate $CaNa_2P_2O_7$ and β-$Ca_3(PO_4)_2$ phases were formed. At 900 °C, only the target phase β-$CaNaPO_4$ was found.

   Heat treatment of cement-salt stone CaNa at a temperature of 500°C led to the formation of a phase composition, which included the β-$CaNaPO_4$, $Ca_{10}(PO_4)_6(OH)_2$, and γ-$Ca_2P_2O_7$ phases. At temperatures of 700 °C and 900 °C, in addition to β-$CaNaPO_4$, phases of β-$Ca_2P_2O_7$, double calcium-sodium pyrophosphate $Na_2CaP_2O_7$ and Na–substituted tricalcium phosphate $Ca_{10}Na(PO_4)_7$ phases were formed in minor quantities.

4. The density of Ca samples increased from 0.52 g/cm³ to 0.59 g/cm³ with an increase in firing temperature from 500 °C to 900 °C or from 41.8 % to 60 % relatively to the density of β-$Ca_2P_2O_7$ equal to 3.09 g/cm³. The shrinkage of the Ca samples was 2.5 % and 3.5 % at 500 °C and 900 °C, respectively.

   With an increase in firing temperature from 500 °C to 900 °C, the density of Na samples increased from 0.56 g/cm³ to 0.94 g/cm³ or from 18 % to 30.2% relatively to the density of β-$CaNaPO_4$ equal to 3.11 g/cm³. The shrinkage of the Na samples was 2.7 % and 18.5 % at 500 °C and 900 °C, respectively.

The density of CaNa samples increased from 0.9 g/cm^3 to 1.43 g/cm^3 or from 28.9 % to 45.9 % relatively to the density of β-CaNaPO$_4$ equal to 3.11 g/cm^3. The shrinkage of the CaNa samples was 4.4 % and 20.1 % at 500 °C and 900 °C, respectively.

5. Thus, ceramic materials in Na_2O-CaO-P_2O_5 system developed here, consisting of biocompatible and bioresorbable β-CPP β-$Ca_2P_2O_7$, β-sodium rhenanite β-CaNaPO$_4$, double calcium-sodium pyrophosphate $Na_2CaP_2O_7$, and Na–substituted tricalcium phosphate $Ca_{10}Na(PO_4)_7$ phases can be used in regenerative methods for the treatment of bone tissue defects.

References

1. Tavoni, M.; Dapporto, M.; Tampieri, A.; Sprio, S. Bioactive calcium phosphate-based composites for bone regeneration. *J. Compos. Sci.* **2021**, *5*, 227. https://doi.org/10.3390/jcs5090227
2. Kanazawa, T. *Inorganic Phosphate Materials*; Elsevier Science Ltd.: Oxford, UK, 1989; 306p.
3. Bohner, M.; Santoni, B.L.G.; Dobelin, N. β-tricalcium phosphate for bone substitution: Synthesis and properties. *Acta Biomater.* **2020**, *113*, 23–41. https://doi.org/10.1016/j.actbio.2020.06.022
4. Eliaz, N.; Metoki, N. Calcium phosphate bioceramics: A review of their history, structure, properties, coating technologies and biomedical applications. *Materials* **2017**, *10*, 334. https://doi.org/10.3390/ma10040334
5. Toshev, O.; Safronova, T.; Kaimonov, M.; Shatalova, T.; Klimashina, E.; Lukina, Y.; Malyutin, K.; Sivkov, S. Biocompatibility of ceramic materials in $Ca_2P_2O_7$–$Ca(PO_3)_2$ system obtained via heat treatment of cement-salt stone. *Ceramics.* **2022**, *5*, 516–532. https://doi.org/10.3390/ceramics5030039
6. Safronova, T.; Kiselev, A.; Selezneva, I.; Shatalova, T.; Lukina, Y.; Filippov, Y.; Toshev, O.; Tihonova, S.; Antonova, O.; Knotko, A. Bioceramics based on β-calcium pyrophosphate. *Materials* **2022**, *15*, 3105. https://doi.org/10.3390/ma15093105
7. Safronova, T.V.; Mukhin, E.A.; Putlyaev, V.I.; Knotko, A.V.; Evdokimov, P.V.; Shatalova, T.B.; Filippov, Y.Y.; Sidorov, E.A.; Karpushkin, E.A. Amorphous calcium phosphate powder synthesized from calcium acetate and polyphosphoric acid for bioceramics application. *Ceram. Int.* **2017**, *43*, 1310–1317. https://doi.org/10.1016/j.ceramint.2016.10.085
8. Yuan, Y.; Yuan, Q.; Wu, C.; Ding, Z.; Wang, X.; Li, G.; Gu, Z.; Li, L.; Xie, H. Enhanced osteoconductivity and osseointegration in calcium polyphosphate bioceramic scaffold via lithium doping for bone regeneration. *ACS Biomater. Sci. Eng.* **2019**, *5*, 5872–5880. https://doi.org/10.1021/acsbiomaterials.9b00950
9. Orlov, N.K.; Putlayev, V.I.; Evdokimov, P.V.; Safronova, T.V.; Garshev, A.V.; Milkin, P.A. Composite bioceramics engineering based on analysis of phase equilibria in the $Ca_3(PO_4)_2$-CaNaPO$_4$-CaKPO$_4$ system. *Inorg. Mater.* **2019**, *55*, 516–523. https://doi.org/10.1134/S0020168519050157
10. Orlov, N.; Kiseleva, A.; Milkin, P.; Evdokimov, P.; Putlayev, V.; Günster, J.; Biesuz, M.; Sglavod, V.M.; Tyablikov, A. Sintering of mixed Ca–K–Na phosphates: Spark plasma sintering vs flash-sintering. *Open Ceram.* **2021**, *5*, 100072. https://doi.org/10.1016/j.oceram.2021.100072

11. Safronova, T.V.; Korneichuk, S.A.; Shatalova, T.B.; Lukina, Y.S.; Sivkov, S.P.; Filippov, Y.; Krut'ko, V.K.; Musskaya, O.N. $Ca_2P_2O_7$–$Ca(PO_3)_2$ ceramic obtained by firing β-tricalcium phosphate and monocalcium phosphate monohydrate based cement stone. *Glass Ceram.* **2020**, 77, 165–172. https://doi.org/10.1007/s10717-020-00263-y

12. Safronova, T.V.; Shatalova, T.B.; Filippov, Y.; Krut'ko, V.K.; Musskaya, O.N.; Safronov, A.S.; Toshev, O.U. Ceramics in the $Ca_2P_2O_7$–Ca $(PO_3)_2$ system obtained by annealing of the samples made from hardening mixtures based on calcium citrate tetrahydrate and monocalcium phosphate monohydrate. *Inorg. Mater.: Appl. Res*. **2020**, *11*, 777–786. https://doi.org/10.1134/S2075113320040334

13. Safronova, T.V.; Lukina, Y.S.; Sivkov, S.P.; Toshev, O.U.; Kazakova, G.K.; Shatalova, T.B.; Filippov, Ya.Yu.; Malyutin K.V.; Aziziyan-Kalandarag, Ya. Ceramics based on calcium pyrophosphate, obtained by annealing cement stone. *Tehknika Tehnol. Silikatov.* **2020**, *27*, 17–20. https://elibrary.ru/item.asp?id=44820756

14. Zhou, H.; Yang, L.; Gbureck, U.; Bhaduri, S.B.; Sikder, P. Monetite, an important calcium phosphate compound–Its synthesis, properties and applications in orthopedics. Acta Biomaterialia **2021**, 127, 41–55. https://doi.org/10.1016/j.actbio.2021.03.050.

15. Toshima, T., Hamai, R., Tafu, M., Takemura, Y., Fujita, S., Chohji, T., S. Tanda,S. Li, Qin, G.W. Morphology control of brushite prepared by aqueous solution synthesis. J. Asian Ceram. Soc., 2014, 2(1), 52-56. https://doi.org/10.1016/j.jascer.2014.01.004

16. Safronova, T.V., Sadilov, I.S., Chaikun, K.V., Shatalova, T.B., Filippov, Ya.Yu. Synthesis of Monetite from Calcium Hydroxyapatite and Monocalcium Phosphate Monohydrate under Mechanical Activation Conditions. *Russ. J. Inorg. Chem.* **2019**, *64*, 1088–1094. https://doi.org/10.1134/S0036023619090171

17. Webb, N.C. The crystal structure of β-$Ca_2P_2O_7$. *Acta Cryst.* **1966**, *21*, 942–948. https://doi.org/10.1107/S0365110X66004225

18. Ding, L.; Wang, H.; Li, J.; Liu, D.; Bai, J.; Yuan, Z.; Yang, J.; Bian, L.; Zhao, X.; Li, B.; Chen, S. Preparation and characterizations of an injectable and biodegradable high-strength iron-bearing brushite cement for bone repair and vertebral augmentation applications. *Biomaterials Science*, **2023**, 11, 96-107. https://doi.org/10.1039/D2BM01535H

19. Navarro, M.; Michiardi, A.; Castano, O.; Planell, J.A. Biomaterials in orthopaedics. *Biomater. Implants Tissue Eng.* **2008**, *5*, 1137–1158. https://doi.org/10.1098/rsif.2008.0151

20. Holland, W.; Rheinberger, V.; Wegner, S.; Frank, M. Needle-like apatite-leucite glass-seramic as a base material for the veneering of metal restorations in dentistry. *J. Mater. Sci. Mater. Med.* **2000**, *11*, 11–17. https://doi.org/10.1023/A:1008977416834

21. Apel, E.; Holland, W.; Rheinberger, V. Bioactive Rhenanite Glass. Ceramic. U.S. Patent 7,074,730, 11 July 2006.

22. Rautaray, H.K.; Dash, R.N.; Mohanty, S.K. Phosphorus supplying power of some thermally promoted reaction products of phosphate rosks. *Fertil. Res.* **1995**, *41*, 67–75. https://doi.org/10.1007/BF00749522

23. Suchanek, W.; Yashima, M.; Kakihana, M.; Yoshimura, M. β-rhenanite (β-$NaCaPO_4$) as weak interphase for hydroxyapatite ceramics. *J. Eur. Ceram. Soc.* **1998**, *18*, 1923–1929. https://doi.org/10.1016/S0955-2219(98)00131-9

24. Ramselaar, M.M.A.; Van Mullem, P.J.; Kalk, W.; Driessens, F.C.M.; Dewijn, J.R.; Stols, A.L.H. In vivo reactions to paniculate rhenanite and particulate hydroxyapatite after implantation in tooth sockets. *J. Mater. Sci. Mater. Med.* **1993**, *4*, 311–317. https://doi.org/10.1007/BF00122287

25. Glasser, F.P.; Gunawardane, R.P. Fertilizer Material from Apatite. U.S. Patent 4,363,650, 14 December 1982.

26. Toshev, O.U.; Safronova, T.V.; Kazakova, G.K.; Shatalova, T.B.; Boytsova, O.V.; Lukina, Y.S.; Sivkov, S.P. Ceramics based on sodium rhenanite $CaNaPO_4$, obtained via firing of composite cement-salt stone. *J. Compos. Sci*. **2022**, *6*, 314. https://doi.org/10.3390/jcs6100314

27. Sventskaya, N.V.; Lukina, Y.S.; Larionov, D.S.; Andreev, D.V.; Sivkov, S.P. 3D-matrix based on bioactive glass and calcium phosphates with controllable resorption rate for bone tissue replacement. *Glass Ceram.* **2017**, *73*, 342–347. https://doi.org/10.1007/s10717-017-9886-3

28. Knotts, R.; Jalota, S.; Bhaduri, S.; Tas, A. Synthesis of Rhenanite (β-$NaCaPO_4$)-Apatitic Calcium Phosphate Biphasics for Skeletal Repair. *Advances in Bioceramics and Porous Ceramics: Ceramic Engineering and Science Proceedings*, **2009**, 29, 151-64.

29. Kaimonov, M.; Safronova, T.; Shatalova, T.; Filippov, Y.; Tikhomirova, I.; Lukina, Y. Composite Ceramics Based on Pastes Including Tricalcium Phosphate and an Aqueous Solution of Sodium Silicate. *J. Compos. Sci.* **2022**, 6, 267. https://doi.org/10.3390/jcs6090267

30. Golubchikov, D.; Safronova, T.V.; Nemygina, E.; Shatalova, T.B.; Tikhomirova, I.N.; Roslyakov, I.V.; Khayrutdinova, D.; Platonov, V.; Boytsova, O.; Kaimonov, M.; Firsov, D.A.; Lyssenko, K.A. Powder Synthesized from Aqueous Solution of Calcium Nitrate and Mixed-Anionic Solution of Orthophosphate and Silicate Anions for Bioceramics Production. *Coatings.* **2023**, 13, 374. https://doi.org/10.3390/coatings13020374

31. ICDD. *International Centre for Diffraction Data*; PDF-4+ 2010 (Database); Kabekkodu, S., Ed.; ICDD: Newtown Square, PA, USA, 2010. Available online: https://www.icdd.com/pdf-2/ (accessed on 20 February 2022).

32. Minh, D.P.; Lyczko, N.; Sebei, H.; Nzihou, A.; Sharrock, P. Synthesis of calcium hydroxyapatite from calcium carbonate and different orthophosphate sources: A comparative study. *Mater. Sci. Eng.: B.* **2012**, *177*, 1080–1089. https://doi.org/10.1016/j.mseb.2012.05.007

33. Ren, D.; Ruan, Q.; Tao, J.; Lo, J.; Nutt, S.; Moradian-Oldak, J. Amelogenin affects brushite crystal morphology and promotes its phase transformation to monetite. *Cryst. Growth Desi.* **2016**, *16*, 4981–4990. https://doi.org/10.1021/acs.cgd.6b00569

34. Hurle, K.; Oliveira, J.M.; Reis, R.L.; Pina, S.; Goetz-Neunhoeffer, F. Ion-doped brushite cements for bone regeneration. *Acta Biomater.* **2021**, *123*, 51–71. https://doi.org/10.1016/j.actbio.2021.01.004

35. Safronova, T.V.; Shatalova, T.B.; Tikhonova, S.A.; Filippov, Y.Y.; Krut'ko, V.K.; Musskaya, O.N.; Kononenko, N.E. Synthesis of calcium pyrophosphate powders from phosphoric acid and calcium carbonate. *Inorg. Mater. Appl. Res.* **2021**, *12*, 986–992. https://doi.org/10.1134/S2075113321040353

36. Prihanto, A.; Fitriyana, D.F.; Muryanto, S.; Masykur, I.; Ismail, R.; Jamari, J.; Bayuseno, A.P. Aqueous crystallization of monocalcium phosphate monohydrate with green mussel shells (*Verna piridis*) for calcium sources. *J. Environ. Chem. Eng.* **2021**, *9*, 106913. https://doi.org/10.1016/j.jece.2021.106913

37. Jinawath, S.; Pongkao, D.; Suchanek, W.; Yoshimura, M. Hydrothermal synthesis of monetite and hydroxyapatite from monocalcium phosphate monohydrate. *Int. J. Inorg. Mater.* **2001**, *3*, 997–1001. https://doi.org/10.1016/S1466-6049(01)00199-4

38. Sarda, S.; Fernández, E.; Nilsson, M.; Balcells, M.; Planell, J.A. Kinetic study of citric acid influence on calcium phosphate bone cements as water-reducing agent. *J. Biomed. Mater. Res.* **2002**, *61*, 653–659. https://doi.org/10.1002/jbm.10264

39. Mansour, S.A.A. Thermal decomposition of calcium citrate tetrahydrate. *Thermochim. Acta* **1994**, *233*, 243–256. https://doi.org/10.1016/0040-6031(94)85118-2

40. Toshev, O.U., Safronova, T.V., Mironova, Y.S., Matveeva, A.S., Shatalova, T.B., Filippov, Ya.Yu., Knotko, A.V., Akhmedov, M.R., Kukueva, E.V., Lukina Yu.S. Ultraporous Submicron-Grained β-Ca$_3$(PO$_4$)$_2$ - Based Ceramics. *Inorg. Mater.* **2022**, 58, 1208–1219. https://doi.org/10.1134/S0020168522110140